Journal of King Saud University – Science 29 (2017) 455–461

Contents lists available at ScienceDirect

Journal of King Saud University – Science

journal homepage: www.sciencedirect.com

Processing of Zn-3Mg alloy by equal channel angular pressing for biodegradable metal implants

Murtala Sule Dambatta [a,b], Sudin Izman [b,*], Denni Kurniawan [b,c], Hendra Hermawan [d,*]

[a] Department of Mechanical Engineering, Kano University of Science and Technology, Kano State, Nigeria
[b] Faculty of Mechanical Engineering, Universiti Teknologi Malaysia, Johor Bahru 81310, Malaysia
[c] Department of Mechanical Engineering, Curtin University, Malaysia, Miri 98009, Malaysia
[d] Department of Mining, Metallurgical and Materials Engineering & CHU de Québec Research Center, Laval University, Quebec City G1V0A6, Canada

ARTICLE INFO

Article history:
Received 17 April 2017
Accepted 27 July 2017
Available online 29 July 2017

Keywords:
Biodegradable metals
Corrosion
ECAP
Grain size
Mechanical
Zinc alloy

ABSTRACT

Zn-based alloys have been studied as new biodegradable metals owing to its slower corrosion rate compared to Mg-based alloys and its high potential for mechanical properties improvement. The present work attempts to improve mainly the mechanical properties of a eutectic Zn-3Mg alloy via equal channels angular pressing (ECAP). Cast Zn-3Mg alloy was homogenized at 370 °C for 15 h and quenched in water before subjected to 2 steps ECAP process. Results showed that the process decreases the alloy's grain size from 48 μm in the as cast to 1.8 μm after 2-passes of ECAP. A remarkably increase of yield strength, tensile strength and elongation was achieved from 65 MPa, 84 MPa and 1.3% (as cast) to 205 MPa, 220 MPa and 6.3% (2-ECAP), respectively. Corrosion rate of the alloy was fairly altered from 0.30 mm/year (as cast) to 0.24 mm/year (2-ECAP). The combination of homogenization and ECAP is therefore viewed as a potential process to improve mechanical properties of Zn-Mg alloys.

1. Introduction

Biodegradable metals have been studied as ideal materials for new generation of temporary load bearing medical implants owing to its combination of strength and biodegradability, which is superior to biodegradable polymers and ceramics (Zheng et al., 2014; Nasution and Hermawan, 2016). Magnesium (Mg)- and iron (Fe)-based alloys are the two classes of biodegradable metals mostly studied for those purposes and have been used to for making endovascular stents and bone pins and screws (Wu et al., 2012; Haude et al., 2016; Lee et al., 2016). Their mechanical properties, corrosion behavior and biocompatibility have been extensively investigated and improved to suit closely to the clinical requirements. However, in the in vivo setting, Fe-based alloys exhibit slow corrosion rate whilst most Mg-based alloys degrade too rapidly (Drynda et al., 2015; Hofstetter et al., 2015). Apart of the works to improve the corrosion behavior of these two classes of alloys, alternatively, zinc (Zn)-based alloys have recently been proposed as new potential biodegradable metals (Vojtěch et al., 2011; Bowen et al., 2013; Mostaed et al., 2016). Zinc is an essential element for humans as it supports the function of many enzymes, regulates inflammatory reactions and enhances bioactivity of bone cells (Fosmire, 1990). The cytocompatibility of Zn-based alloys have been studied against various cells such as fibroblast, osteoblast and osteosarcoma giving the evidence of the alloys potentiality for bone implant applications (Murni et al., 2015; Shearier et al., 2016; Shen et al., 2016).

However, the low strength of Zn (~20 MPa) and its brittleness are considered far from ideal for fabricating load bearing implants. But once alloyed Zn, such as Zn-1Mg, the alloy can reach a tensile strength of 150 MPa that is superior strength to some Mg-based alloys (Vojtěch et al., 2011; Gong et al., 2015). Alloying Zn with less than 4 wt% Mg was also reported to enhance the corrosion resistance (Prosek et al., 2008). Alloying of Zn via casting usually results into the occurrence of micro-segregation and thereby additional processes such as heat treatment and extrusion have been used to eliminate this defect (Gong et al., 2015; Dambatta et al., 2015). After being subjected to extrusion, Zn-1Mg alloy exhibited an improvement on both tensile strength and elongation from

* Corresponding authors.
E-mail addresses: izman@mail.fkm.utm.my (S. Izman), hendra.hermawan@gmn.ulaval.ca (H. Hermawan).
Peer review under responsibility of King Saud University.

Production and hosting by Elsevier

http://dx.doi.org/10.1016/j.jksus.2017.07.008
1018-3647/

about 150 MPa and 1% to 200 MPa and 10%, respectively (Gong et al., 2015). Further improvement to the mechanical properties should be made possible via severe plastic deformation processes, such as high pressure torsion and equal channel angular pressing (ECAP). These processes have been used to transform micro to ultra-fine or nano-size grains of various Zn-Al alloys for industrial applications (Pürçek, 2005; Al-Maharbi et al., 2010; Aydın, 2012). During ECAP, a metal is subjected to an intense plastic straining through simple shear without corresponding change in its cross-sectional dimension. It was found to be capable of providing an increase in both strength and ductility as observed for cast Zn-Al alloys due to microstructural refinement and elimination or reduction of cast dendritic structure as well as casting defects (Al-Maharbi et al., 2010; Aydın, 2012). This process should be an ideal technique to improve the mechanical properties of cast Zn-Mg alloys specifically targeted for biomedical applications. Therefore, the present study employs an ECAP process to a homogenized cast Zn-3Mg alloy and is aimed mainly to show an improvement in the mechanical properties of the alloy. The Zn-3Mg alloy was selected based on the expectation for facilitating the ECAP at lower processing temperature as 3 wt% Mg is a eutectic composition having the lowest melting temperature (364 °C) in the Zn-Mg system (Vojtěch et al., 2011) and for maintaining corrosion resistance that was found to decrease in Zn-Mg alloys with lower Mg content after subjected to additional thermomechanical processing (Prosek et al., 2008).

2. Materials and methods

2.1. Materials preparation and ECAP process

A Zn-3Mg alloy (3 wt% Mg) was prepared from pure Zn (99.99% purity) and pure Mg (99.95% purity) ingots (Goodfellow Inc., UK) using a conventional casting method. The ingots were melted at 550 °C using an induction furnace protected by a flow of argon. The molten metal was mechanically stirred for 2 min before cast into a preheated (~150 °C) rectangular shaped cast iron mould and then cooled to room temperature. Billets having dimension of 8 × 8 × 120 mm were cut out from the cast and subsequently homogenized under vacuum at 370 °C for 15 h followed by water quenching. The billets were then subjected to ECAP at one pass (1-ECAP) and two passes (2-ECAP) using a hardened steel dies having 8 × 8 mm of square channel section and intersection angle of 120°. A progressive pressing force was applied at a constant speed of 1 mm/s using an Instron-5569 universal testing machine. Molybdenum disulfide was used as the solid lubricant to reduce friction between the die and the billets. The ECAP dies was heated at 200 °C to allow a smooth passage of the billets through the channel without cracking. Cracks were observed on billets processed at 100–190 °C while increasing the temperature above 210 °C led to partial melting of the billets.

2.2. Characterization and mechanical testing

All samples for microstructure observation were longitudinally cut (parallel to the ECAP direction). Their microstructure was observed under an optical microscope (Nikon Microphot-FXL, Japan) after being ground, polished with diamond suspension (from 3 μm to 1 μm) and colloidal silica suspension (0.04 μm), and finally etched with acid solution containing 50 g CrO_3, 15 g Na_2SO_4 in 1 L distilled water at 80 °C. The optical micrographs were used to measure the average grain size and percentage of porosity by using image analysis software (Microvisual Advance, IMT iSolution, Canada) with three replications. The average grain size was measured using ferret diameter which is the average caliper lengths of the grains. Microstructural observation and elemental analysis at higher magnification were done by using a Field Emission Scanning Electron Microscope (FESEM, Zeiss Supra VP35, Germany) equipped with Energy Dispersive X-ray Spectroscopy (EDS, Oxford Instrument, UK). Phase identification was conducted using an X-ray diffraction machine (XRD, Siemens-D500, Germany) with Cu Kα line generated at 40 kV and 35 mA. Further analysis of the XRD pattern was performed to determine the crystallite size of detected phases on both homogenized and ECAP samples using Debye–Scherrer equation: $T = \frac{C\lambda}{B\cos\theta}$, where T is the crystallite size (nm), λ is the wavelength of the X-rays (i.e. 1.541 Å for Cu Kα radiation), C is the shape factor equal to 0.9, θ is the Braggs angle, and B is the full-width at half-maximum (FWHM) of the selected peak (radians). Microhardness measurement was carried out using a Vickers hardness tester (DVK-2 Matsuzawa, Japan) by applying 5 kg load at room temperature for 15 s at five different locations on each polished specimen with three replications. Tensile test was conducted by using a universal testing machine (Instron-5569, Japan) at a constant strain rate of 0.5 mm/min on flat specimens having 9 mm gage length, 40 mm length and 3 mm thickness with at least three replications. The test and the determination of tensile strength, yield strength, maximum elongation and Young's modulus were done in accordance with the ASTM E8M standard (Standard Test Methods for Tension Testing of Metallic Materials).

2.3. Corrosion testing

Corrosion behavior of the metal samples was assessed using both simple immersion and electrochemical polarization methods. Test solution was prepared based on Kokubo's simulated body fluid (SBF) containing the following ions in mmol/L: 142 Na^+, 5 K^+, 2.5 Ca^+ 1.5 Mg^+, 4.2 HCO_3^-, 103 Cl^-, 1 HPO_4^{2-} and 0.5 SO_4^{2-} at adjusted pH of 7.4 (Kokubo and Takadama, 2006). For immersion test, metal samples of 7.9 × 7.8 × 3 mm were prepared, weighed and immersed (in triplicate) in stagnant SBF solution at 37 ± 1 °C. The samples were removed after 21 days and rinsed with distilled water then allowed to dry at room temperature. Prior to corrosion product cleaning, surface morphology, elemental compositions and formed corrosion products were analysed and evaluated. Corrosion products were then removed from the samples by a chemical cleaning as specified in the ASTM G1 standard (Standard Practice for Preparing, Cleaning, and Evaluating Corrosion Test Specimens). Cleaned samples were then weighed to determine the weight loss. A flame atomic absorption spectrometry (Perkin Elmer, HGA 9000 model) technique was used to determine the concentration of Zn and Mg ions released by the samples into the SBF solution during the immersion test period. Corrosion rate of the samples was calculated by using equation: Corrosion rate = (KW)/(ATD), where the coefficient K = 8.76 × 10^4, W is the weight loss (g), A is the sample area exposed to the SBF solution (cm^2), T is the exposure time (h) and D is the density of the exposed material (g/cm^3). Electrochemical corrosion test was conducted using potentiodynamic polarization and electrochemical impedance spectroscopy (EIS) methods by means of a potentiostat (VersaStat-3, Princeton Applied Research, US). The three-electrode system was used with the metal sample; graphite rod and saturated calomel electrode (SCE) served as the working, counter and reference electrodes, respectively. The test was carried out at 37 °C after 15 min stabilization time at the open-circuit potential (OCP) at a potential range from −200 to +700 mV against the OCP and a scan rate of 2 mV/s. Tafel fitting as suggested by Atrens et al. (2011) was used to approximate the corrosion potential and corrosion current which then used to calculate the corrosion rate of the alloy (CR) using the equation: $CR = 3.27 * 10^{-3} \frac{i_{corr} EW}{\rho}$, where EW is equivalent weight and ρ is density of the alloy.

3. Results

3.1. Microstructure observation

Fig. 1 shows microstructure of the as cast, homogenized and ECAP samples of Zn-3Mg alloy. The as cast alloy consisted of Zn-rich dendrites dispersed in segregated form within the Mg_2Zn_{11} phase (Fig. 1a). The dendrites were mostly dissolved during homogenization (Fig. 1b), with some of undissolved dendrites appear to have been experienced breakdown and transformation into connected precipitates. The 1-ECAP alloy possesses a near equiaxial microstructure with finer grain size but some elongated dendrites are still observed (Fig. 1c). In 2-ECAP alloy, the grain size is further refined with microstructure composed of complete equiaxed grains (Fig. 1d).

Table 1 details the results of grain size measurement of the alloy. In average, the grain size was decreased progressively from about 48 μm (as cast) to 30 μm (homogenized), 2.3 μm (1-ECAP) and 1.8 μm (2-ECAP). The grain size is distributed within a range of 30–150 μm (as cast) to 20–80 μm (homogenized) and 0.9–12 μm (2-ECAP) indicating the effectiveness of the process in refining the grains. Furthermore, percentage of porosity was also measured and shows a decrease from about 7% (as cast) to 4% (homogenized) and 0.04% (1-ECAP) till 0.02% (2-ECAP) indicating the effectiveness of the process in eliminating the defect generated by the primary process (casting).

Fig. 2a shows XRD pattern of homogenized, 1-ECAP and 2-ECAP Zn-3Mg alloy detecting the presence of hexagonal structure of Zn-rich phase (JCPDS: 00-004-0831) and cubic structure of Mg_2Zn_{11} phase (JCPDS: 03-065-1853). The study by Li et al. (2003) reported the presence of intermetallic phases of Zn and Mg_2Zn_{11} which formed above 325 °C during casting of Zn and Mg metals. There was a decrease of crystalline size of homogenized Zn-3Mg alloy after subjected to ECAP process. The crystallite size of Zn-rich phase on homogenized, 1-ECAP and 2-ECAP sample was 24.86 nm, 10.36 nm and 9.51 nm whilst for Mg_2Zn_{11} phase was 14.30 nm, 10.75 nm and 10.45 nm, respectively.

3.2. Mechanical testing

Fig. 2b shows tensile curves of the alloys at different metallurgical conditions indicating an obvious improvement on tensile

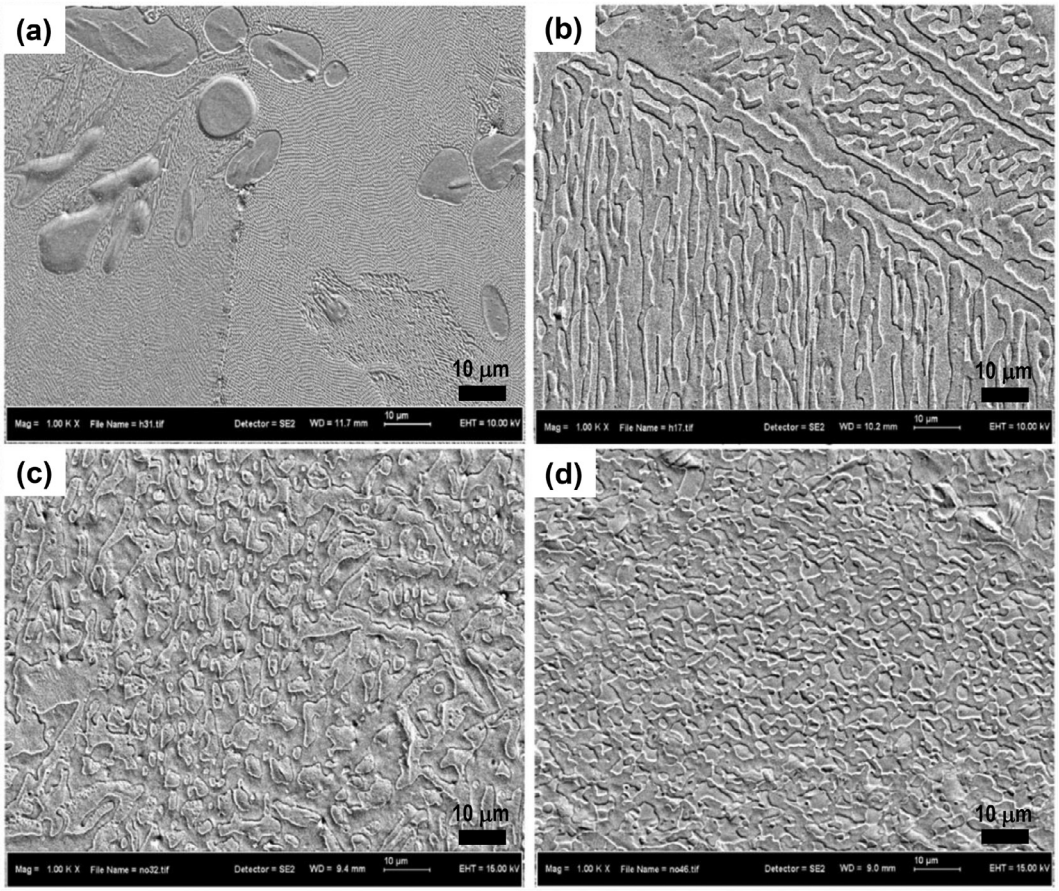

Fig. 1. Zn-3Mg alloy microstructure: (a) as cast, (b) homogenized, (c) 1-ECAP, and (d) 2-ECAP.

Table 1
Average grain size of the Zn-3Mg alloy at different metallurgical conditions.

Zn-3Mg alloy	Total grain counted	Porosity area (%)	Average min feret diameter (μm)	Average max feret diameter (μm)	Mean feret diameter (μm)
As cast	371	6.57	40 ± 0.6	58.1 ± 0.9	47.9 ± 0.7
Homogenized	1212	4.01	21.2 ± 0.2	36.4 ± 0.1	29.8 ± 0.1
1-ECAP	1572	0.04	1.7 ± 0.1	2.8 ± 0.4	2.3 ± 0.2
2-ECAP	2659	0.02	1.3 ± 0.3	2.1 ± 0.6	1.8 ± 0.4

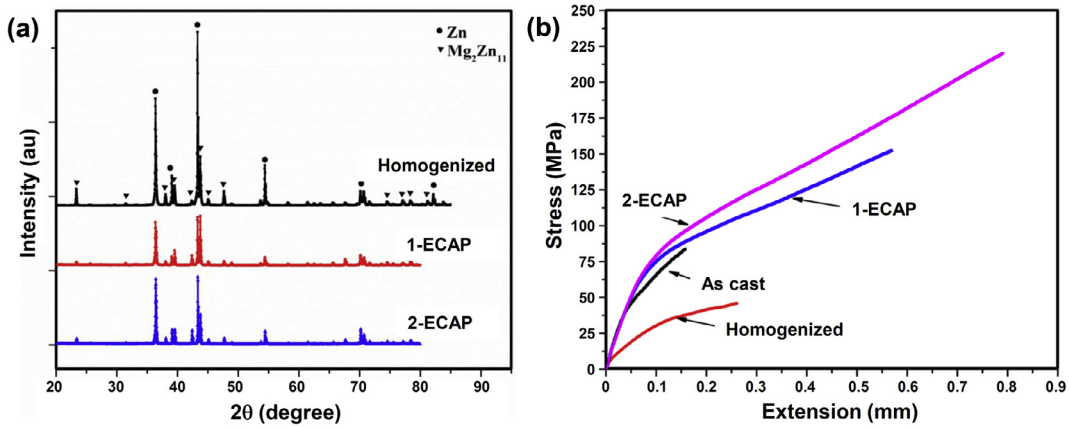

Fig. 2. (a) XRD pattern and (b) tensile curves of the Zn-3Mg alloy samples.

Table 2
Mechanical properties of Zn-3Mg alloy at different metallurgical conditions.

Zn-3Mg alloy	Tensile strength (MPa)	Yield strength (MPa)	Elongation (%)	Young's Modulus (GPa)	Hardness (Hv)
As cast	84 ± 9	65 ± 9	1.3 ± 0.3	132 ± 4	200 ± 7
Homogenized	46 ± 1	36 ± 3	2.1 ± 0.1	84 ± 3	175 ± 8
1-ECAP	153 ± 4	137 ± 2	4.6 ± 0.5	205 ± 9	180 ± 4
2-ECAP	220 ± 3	205 ± 4	6.3 ± 0.9	210 ± 8	186 ± 4

strength as well as elongation of the Zn-3Mn alloy after subjected to ECAP. As detailed in Table 2, an increase in tensile strength, yield strength and elongation was achieved by the 2-ECAP sample at about 160%, 215%, and 400% higher than those of the as cast alloy, respectively. Results from Vickers microhardness measurement indicates a similar trend where hardness decrease from 200 Hv (as cast) to 175 Hv (homogenized) and then a slight increase to 180 Hv (1-ECAP) and 186 Hv (2-ECAP).

Fig. 3 shows fracture surface of the samples after subjected to tensile tests. The morphology of both as cast (Fig. 4a) and homogenized alloy (Fig. 4b) is characterized by a relatively flat facet surface indicating a brittle fracture behavior. More dimples are noticed on the surface of ECAP samples (Fig. 4c–d) indicating a transitional fracture behavior from fully brittle to slightly ductile.

3.3. Corrosion testing

The corrosion rate of homogenized, 1-ECAP and 2-ECAP Zn-3Mg alloy samples after being immersed in the SBF solution for 21 days is listed in Table 3. Corrosion rate of the homogenized sample is similar to that of as cast alloy previously reported (Dambatta et al., 2015). A decrease on the corrosion rate is observed for the ECAP samples and it is supported by the decrease in Zn and Mg ions concentration released from the samples into the SBF solution during the immersion test.

Fig. 4 shows surface morphology of the Zn-3Mg alloy samples after being subjected to the immersion test. A porous corrosion layer dominates the surface morphology of homogenized sample (Fig. 4a). A rather granulated corrosion layer characterizes the surface of 1-ECAP sample (Fig. 4b) which seems different to that of 2-ECAP where crystal-like structure is formed (Fig. 4c). The EDS analysis revealed the presence of Cl, Zn, Mg, Ca, P, and O elements on the corroded surfaces. The XRD pattern (Fig. 4d) further detected the presence of zinc hydroxide [$Zn(OH)_2$] (JCPDS: 38-0385) and hydrozincite [$Zn_5(OH)_6(CO3)_2$] (JCPDS: 54-0047). Previous studies have shown that Zn-Mg alloys (with Mg content of 1–16 wt%) immersed in aggressive chloride containing solution usually formed corrosion products consisting of insoluble hydrozincite [$Zn_5(OH)_6(CO_3)_2$] and traces of simonkolleite [$Zn_5(OH)_8Cl_2{\cdot}H_2O$] (JCPDS: 07-0155) Prosek et al., 2008.

Fig. 5a depicts Nyquist plots of the three Zn-3Mg alloy samples. The plots of ECAP samples indicate the existence of two capacitive loops at high and mid frequencies. Previous studies reported that capacitive loop observed at high frequency corresponds to charge transfer reaction in the electric double layer that occurred at the exposed surface and solution interface (Prosek et al., 2008; Zucchi et al., 2006). Fig. 5b shows potentiodynamic polarization curves of the alloy that indicate a little change to corrosion potential of the alloy regardless their metallurgical condition resulting into a narrow range of corrosion rates at around 0.24–0.30 mm/year (Table 4). The dielectric properties of the layer were analyzed by proposing an equivalent circuit (inset Fig. 5a) and the values are presented in Table 4. In addition to the presence of Warburg impedance, the charge transfers resistance (R_{ct}) value of 1-ECAP is higher than that of 2-ECAP samples. Conversely, homogenized sample gives the least value of R_{ct} compared to ECAP samples. It is well established that higher R_{ct} value corresponds to higher corrosion resistance (Rondelli et al., 2005).

4. Discussion

4.1. Microstructure evolution and mechanical properties

The dendritic structure of the as cast Zn-3Mg alloy was dissolved during homogenization and transformed into equiaxed grains during the 2 steps ECAP process (Fig. 1). The grain size refinement during ECAP is attributed to the interaction of shear and recrystallization that occurs along the equal channel intersection angle (Verlinden, 2005). The process gives also similar effect on the reduction of casting defects such as porosity. The initial coarse grain size of the as cast alloy was reduced by 96% due to the combining process of homogenization and two passes of ECAP (Table 1). This notable grain refinement can be attributed to the first partial refinement by the homogenization that speeds up the process in ECAP. It was observed that the initial grain size prior to ECAP plays a vital role in controlling the rate of refinement at

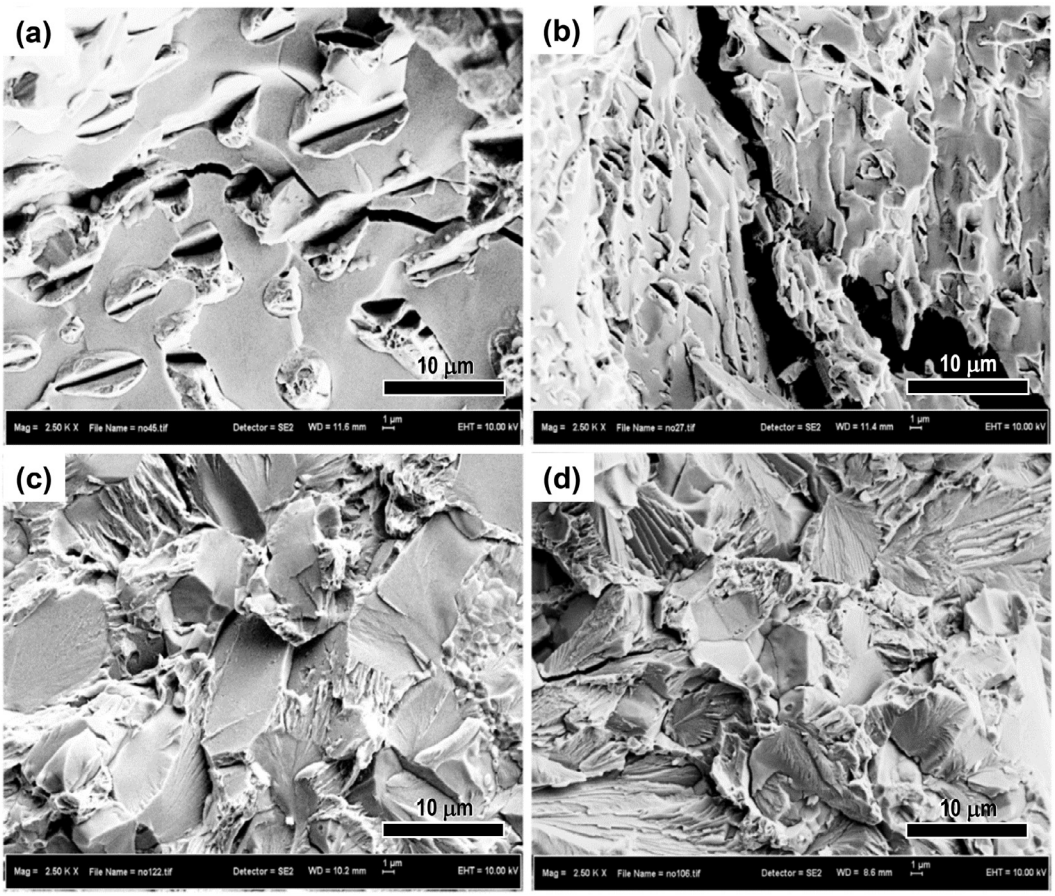

Fig. 3. Fracture surface of Zn-3Mg alloy samples after tensile tests: (a) as cast, (b) homogenized, (c) 1-ECAP, and (d) 2-ECAP.

the final stage of ECAP process (Mostaed et al., 2014). The present combined technique reduces the number of ECAP pass thus potentially reduces production cycle, time and cost. Most of the reported grain size refinement in the range of 1–2 μm for Zn-Al alloys was achieved after conducting 8–12 ECAP passes (Pürçek, 2005; Al-Maharbi et al., 2010; Aydın, 2012). In addition, there is still a room for optimization such as by progressively decreasing the ECAP temperature in the range of 190–210 °C to allow higher plastic straining and add more passes without causing cracks. This manipulation was found useful in the ECAP process for Mg-Zn alloy (Mostaed et al., 2014). The XRD pattern reveals that there is no major variation in phase formation between the homogenized and the ECAP Zn-3Mg alloy. Phase identification on both conditions indicates the presence of Zn-rich and Mg_2Zn_{11} phases (Fig. 2a). The crystallite size of Zn-rich and Mg_2Zn_{11} phases of homogenized alloy decreases after being processed through ECAP which correlates very well with the SEM observation on the reduction of grains size (Fig. 1). Similarly, remarkable reduction of porosity was observed after 2-ECAP passes. The samples processed up to 2-ECAP passes exhibit a reduction of percentage porosity of about 300 times compared to as cast sample (Table 1). This implies that reduction of the observed porosity after homogenization followed by ECAP process contributes also toward improving the alloy's ductility. Therefore, as expected the refined grains structure improves mechanical properties of the alloy (Fig. 2b). The combined homogenization and the two passes of ECAP increases both strength and ductility (Table 2), in contrast with the results obtained by strain hardening treatment such as extrusion that increase the strength in expense of ductility. The increase in strength and ductility at the same time could be attributed to fine microstructure and high number of grains size that lead to increase of volume density of high-angle grain boundaries in the Zn-3Mg alloy after ECAP. The grain boundaries impinge dislocation movement and hence increase the alloy's strength but at the same time the large number of individual grains increases the possibility of slip to occur and hence improves the alloy's ductility (Chuvil'Deev et al., 2004; Valiev et al., 2002). The increase of ductility may also be a result of the breakdown and homogenous distribution of hard Mg_2Zn_{11} intermetallic phase in addition to the reduction of porosity. The small change in hardness may indicate a nearly saturated effect of ECAP that leads to no more increase of hardness with additional ECAP passes. This is in consistent with previous finding on Zn-Al alloy subjected to ECAP (Al-Maharbi et al., 2010). The fracture morphology of ECAP samples show a ridge-like features radiating outwards with lesser flat facet area but more dimples for 2-ECAP (Fig. 3). This feature indicates an occurrence of typical brittle fracture that took place with little appreciable deformation (Callister and Rethwisch, 2012). However, the indication of a transitional fracture behavior from full brittle to slight ductile (Fig. 3) correlates very well with the increase of elongation (Fig. 2b).

4.2. Corrosion behavior

The immersion and electrochemical corrosion tests revealed that corrosion rate of homogenized and ECAP samples (0.24–0.30 mm/year) is comparable to that of as cast alloy (0.23 mm/year) Dambatta et al., 2015. This can be attributed to the effect of Mg alloying on the formation of a relatively stable oxide layer on the alloy's surface. In more detail, the results show that both ECAP samples exhibited lower corrosion rate when compared to homog-

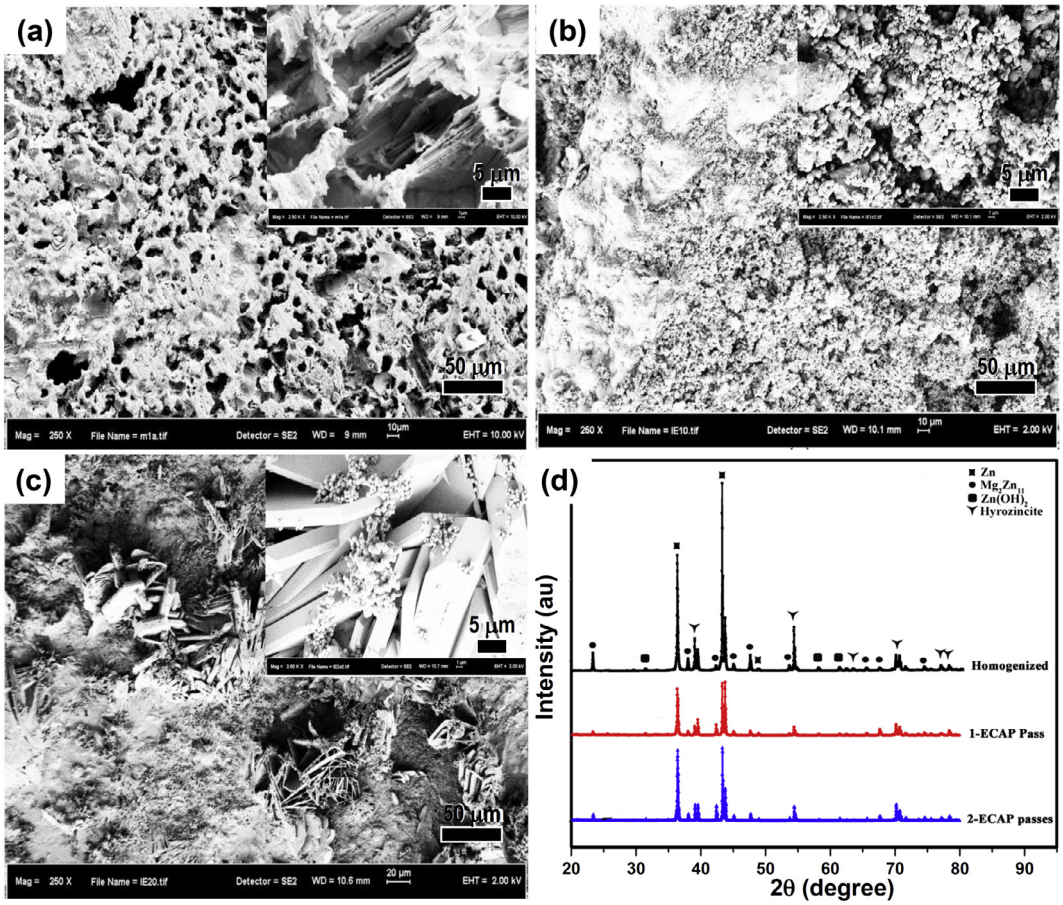

Fig. 4. Surface morphology of: (a) homogenized, (b) 1-ECAP and (c) 2-ECAP samples after immersed in SBF solution for 21 days, and (d) their corresponding XRD pattern.

Table 3
Corrosion rate of the Zn-3Mg alloy and concentration of ions released into the SBF solution.

Zn-3Mg samples	Corrosion rate (mm/year)	Zn ion (mg/l)	Mg ion (mg/l)
Homogenized	0.25	1.14	38.99
1-ECAP	0.18	0.86	25.77
2-ECAP	0.19	0.91	28.75

enized sample (Table 3). This could be attributed to the uniform distribution of the Mg_2Zn_{11} intermetallic phase after ECAP in addition a homogenous grain structure. A slight increase in corrosion rate of 2-ECAP compared to 1-ECAP (Table 4) can be related to the existence of finer grains size observed in the microstructure of 2-ECAP sample (Fig. 1d) leading to the formation of a less resistive corrosion layer (Table 4). The measured slight higher ions concentration released from 2-ECAP compared 1-ECAP sample (Table 3) further supports this finding. This is in agreement with previous corrosion study that reported that samples with fine-grained microstructure may likely to corrode faster than those consisted of coarse-grained microstructure (Kutniy et al., 2009). The analysis on EIS result indicates the presence of a more resistive corrosion layer formed on both ECAP samples compared to the homogenized sample (Fig. 5a and Table 4). The presence of mid-frequency capacitive loop on ECAP samples implies corrosion

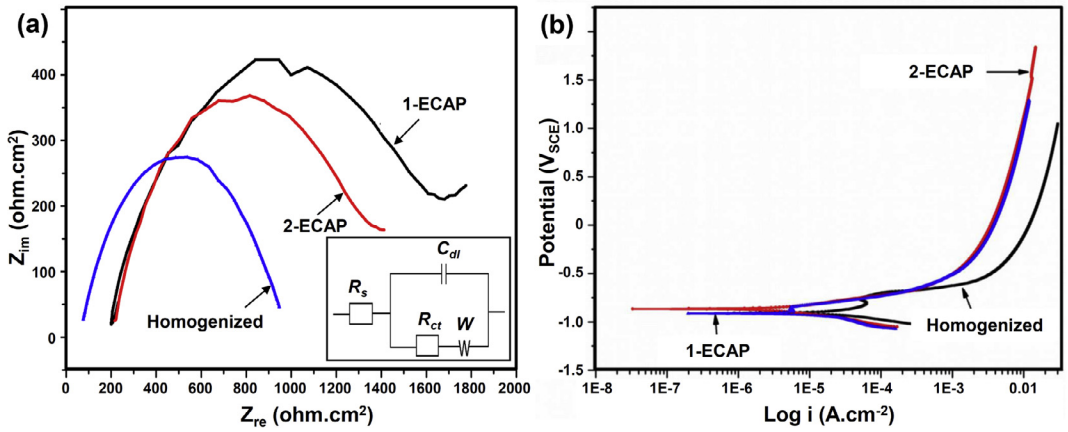

Fig. 5. (a) Nyquist plots and (b) polarization curves of homogenized, 1-ECAP, and 2-ECAP Zn-3Mg alloy samples tested in SBF solution at 37 °C.

Table 4
Corrosion parameters derived from the EIS and polarization curves.

Zn-3Mg alloy	EIS				Polarization		
	R_s (ohm)	C_{dl} (10^{-7} F)	R_{ct} (ohm)	W ($S.s^{1/2}$)	E_{corr} (mV)	i_{corr} ($\mu A/cm^2$)	CR (mm/year)
Homogenized	109.5	3.02	389	–	−902	3.4	0.3
1-ECAP	553.2	11.41	2560	4.04×10^{-4}	−865	2.7	0.24
2-ECAP	355.5	9.81	1135	–	−893	3.2	0.28

mechanism occurred due to mass transport in solid phase such as diffusion of ions through oxide layers (Walter and Kannan, 2011). Conversely, the absence of mid frequency loop was noticed on the homogenized sample which could be attributed to poorly formed protective layer as observed on the surface morphology (Fig. 4a). The corrosion layer, as revealed by the XRD analysis (Fig. 4d), is composed of hydrozincite where its formation may be related to high local pH magnesium rich corrosion product. Earlier investigation reported a stable hydrozincite at higher pH value (Lindström et al., 2002; Volovitch et al., 2009).

5. Conclusion

A Zn-3Mg alloy was processed through a hybrid process of homogenization followed by 2 passes of ECAP leading to a grain size refinement from 48 μm (as cast) to 1.8 μm (2-ECAP). This refined microstructure finally leads to a notable improvement on both tensile strength and ductility of the alloy from 84 MPa and 1.3% (as cast) to 220 MPa and 6.3% (2-ECAP), respectively. The corrosion tests revealed that fine grain structure fairly enhances corrosion resistant of the ECAP sample which is attributed to the homogenous microstructure, low casting defect and uniform distribution of phases. Hence, combination of homogenization and ECAP is therefore viewed as a potential process to improve mechanical and corrosion properties of Zn-Mg alloys for biodegradable metal implants.

Acknowledgements

The authors acknowledge the financial support from the Malaysian Ministry of Education and the Natural Sciences and Engineering Research Council of Canada (NSERC). This paper is dedicated to the memory of our wonderful co-worker, Bashir Yahaya, who passed away in the time we were revising the manuscript. This work is part of international research collaboration between Laval University, Canada and Universiti Teknologi Malaysia, Malaysia.

References

Al-Maharbi, M., Karaman, I., Purcek, G., 2010. Flow response of a severe plastically deformed two-phase zinc–aluminum alloy. Mater. Sci. Eng., A 527, 518–525.
Atrens, A., Liu, M., Zainal Abidin, N.I., 2011. Corrosion mechanism applicable to biodegradable magnesium implants. Mater. Sci. Eng., B 176, 1609–1636.
Aydın, M., 2012. High-cycle fatigue behavior of severe plastically deformed binary Zn–60Al alloy by equal-channel angular extrusion. J. Mater. Process. Technol. 212, 1780–1789.
Bowen, P.K., Drelich, J., Goldman, J., 2013. Zinc exhibits ideal physiological corrosion behavior for bioabsorbable stents. Adv. Mater. 25, 2577–2582.
Callister, W.D., Rethwisch, D.G., 2012. Fundamentals of Materials Science and Engineering: An Integrated Approach. John Wiley & Sons.
Chuvil'Deev, V., Nieh, T., Gryaznov, M.Y., Sysoev, A., Kopylov, V., 2004. Low-temperature superplasticity and internal friction in microcrystalline Mg alloys processed by ECAP. Scr. Mater. 50, 861–865.
Dambatta, M.S., Izman, S., Kurniawan, D., Farahany, S., Yahaya, B., Hermawan, H., 2015. Influence of thermal treatment on microstructure, mechanical and degradation properties of Zn-3Mg alloy as potential biodegradable implant material. Mater. Des. 85, 431–437.
Drynda, A., Hassel, T., Bach, F.W., Peuster, M., 2015. In vitro and in vivo corrosion properties of new iron-manganese alloys designed for cardiovascular applications. J. Biomed. Mater. Res. B Appl. Biomater. 103, 649–660.
Fosmire, G.J., 1990. Zinc toxicity. Am. J. Clin. Nutr. 51, 225–227.
Gong, H., Wang, K., Strich, R., Zhou, J.G., 2015. In vitro biodegradation behavior, mechanical properties, and cytotoxicity of biodegradable Zn–Mg alloy. J. Biomed. Mater. Res. B Appl. Biomater. 103, 1632–1640.
Haude, M., Ince, H., Abizaid, A., Toelg, R., Lemos, P.A., von Birgelen, C., et al., 2016. Safety and performance of the second-generation drug-eluting absorbable metal scaffold in patients with de-novo coronary artery lesions (BIOSOLVE-II): 6 month results of a prospective, multicentre, non-randomised, first-in-man trial. Lancet 387, 31–39.
Hofstetter, J., Martinelli, E., Weinberg, A.M., Becker, M., Mingler, B., Uggowitzer, P.J., et al., 2015. Assessing the degradation performance of ultrahigh-purity magnesium in vitro and in vivo. Corros. Sci. 91, 29–36.
Kokubo, T., Takadama, H., 2006. How useful is SBF in predicting in vivo bone bioactivity? Biomaterials 27, 2907–2915.
Kutniy, K., Papirov, I., Tikhonovsky, M., Pikalov, A., Sivtzov, S., Pirozhenko, L., et al., 2009. Influence of grain size on mechanical and corrosion properties of magnesium alloy for medical implants. Materialwiss. Werkstofftech. 40, 242–246.
Lee, J.-W., Han, H.-S., Han, K.-J., Park, J., Jeon, H., Ok, M.-R., et al., 2016. Long-term clinical study and multiscale analysis of in vivo biodegradation mechanism of Mg alloy. Proc. Natl. Acad. Sci. 113, 716–721. http://dx.doi.org/10.1073/pnas.1518238113.
Li, Y.B., Bando, Y., Golberg, D., 2003. Mg2Zn11-MgO belt-like nanocables. Chem. Phys. Lett. 375, 102–105.
Lindström, R., Svensson, J.-E., Johansson, L.G., 2002. The influence of salt deposits on the atmospheric corrosion of zinc. The important role of the sodium ion. J. Electrochem. Soc. 149, B57–B64.
Mostaed, E., Hashempour, M., Fabrizi, A., Dellasega, D., Bestetti, M., Bonollo, F., et al., 2014. Microstructure, texture evolution, mechanical properties and corrosion behavior of ECAP processed ZK60 magnesium alloy for biodegradable applications. J. Mech. Behav. Biomed. Mater. 37, 307–322.
Mostaed, E., Sikora-Jasinska, M., Mostaed, A., Loffredo, S., Demir, A., Previtali, B., et al., 2016. Novel Zn-based alloys for biodegradable stent applications: design, development and in vitro degradation. J. Mech. Behav. Biomed. Mater. 60, 581–602.
Murni, N.S., Dambatta, M.S., Yeap, S.K., Froemming, G.R.A., Hermawan, H., 2015. Cytotoxicity evaluation of biodegradable Zn–3Mg alloy toward normal human osteoblast cells. Mater. Sci. Eng., C 49, 560–566.
Nasution, A.K., Hermawan, H., 2016. Degradable biomaterials for temporary medical implants. Adv. Struct. Mater. 58, 127–160. http://dx.doi.org/10.1007/978-3-319-14845-8_6.
Prosek, T., Nazarov, A., Bexell, U., Thierry, D., Serak, J., 2008. Corrosion mechanism of model zinc–magnesium alloys in atmospheric conditions. Corros. Sci. 50, 2216–2231.
Pürçek, G., 2005. Improvement of mechanical properties for Zn–Al alloys using equal-channel angular pressing. J. Mater. Process. Technol. 169, 242–248.
Rondelli, G., Torricelli, P., Fini, M., Giardino, R., 2005. In vitro corrosion study by EIS of a nickel-free stainless steel for orthopaedic applications. Biomaterials 26, 739–744.
Shearier, E.R., Bowen, P.K., He, W., Drelich, A., Drelich, J., Goldman, J., et al., 2016. In vitro cytotoxicity, adhesion, and proliferation of human vascular cells exposed to zinc. ACS Biomater. Sci. Eng. 2, 634.
Shen, C., Liu, X., Fan, B., Lan, P., Zhou, F., Li, X., et al., 2016. Mechanical properties, in vitro degradation behavior, hemocompatibility and cytotoxicity evaluation of Zn–1.2Mg alloy for biodegradable implants. RSC Adv. 6, 86410–86419.
Valiev, R., Alexandrov, I., Zhu, Y., Lowe, T., 2002. Paradox of strength and ductility in metals processed by severe plastic deformation. J. Mater. Res. 17, 5–8.
Verlinden, B., 2005. Severe plastic deformation of metals. Metalurgija 11, 165–182.
Vojtěch, D., Kubásek, J., Šerák, J., Novák, P., 2011. Mechanical and corrosion properties of newly developed biodegradable Zn-based alloys for bone fixation. Acta Biomater. 7, 3515–3522.
Volovitch, P., Allely, C., Ogle, K., 2009. Understanding corrosion via corrosion product characterization: I. Case study of the role of Mg alloying in Zn–Mg coating on steel. Corros. Sci. 51, 1251–1262.
Walter, R., Kannan, M.B., 2011. Influence of surface roughness on the corrosion behaviour of magnesium alloy. Mater. Des. 32, 2350–2354.
Wu, C., Qiu, H., Hu, X., Ruan, Y., Tian, Y., Chu, Y., et al., 2012. Short-term safety and efficacy of the biodegradable iron stent in mini-swine coronary arteries. Chin. Med. J. 126, 4752–4757.
Zheng, Y.F., Gu, X.N., Witte, F., 2014. Biodegradable metals. Mater. Sci. Eng. R: Rep. 77, 1–34.
Zucchi, F., Grassi, V., Frignani, A., Monticelli, C., Trabanelli, G., 2006. Electrochemical behaviour of a magnesium alloy containing rare earth elements. J. Appl. Electrochem. 36, 195–204.